Catenary mechanism in steel columns under extreme lateral loading: A basis for building progressive collapse analysis

Developments in the Built Environment 20 (2024) 100556

Contents lists available at ScienceDirect

Developments in the Built Environment

journal homepage: www.sciencedirect.com/journal/developments-in-the-built-environment

Catenary mechanism in steel columns under extreme lateral loading: A basis for building progressive collapse analysis

Foad Kiakojouri, Valerio De Biagi *

Department of Structural, Geotechnical and Building Engineering (DISEG) - Politecnico di Torino, Torino, Italy

ARTICLE INFO

Keywords:
Catenary effects
Steel column
Progressive collapse
Local damage
Extreme event

ABSTRACT

The studies on progressive collapse have primarily focused on threat-independent methods, wherein a sudden column removal is suggested in codes. However, a real collapse scenario is necessarily threat-dependent. Focusing on blast- and impact-induced progressive collapses, the current study considers cases in which damage is concentrated in a single member, without resulting in complete column loss. It is demonstrated that the progressive collapse performance under specific threats can be better or worse compared to that of sudden column removal. Thus, dynamic column removal does not necessarily guarantee the most critical scenario, as the response in a damaged system can sometimes exceed expectations. A simple analytical model is proposed to describe in detail the observed phenomena and emphasizes the development of catenary forces in the column under lateral extreme loading scenarios. The results provide a deeper insight into the progressive collapse performance of frame systems and the involved member-level resisting mechanisms.

1. Introduction

Structural collapse is the foremost concern for any structural engineer. Among various collapse mechanisms, progressive collapse, where an initial local failure spreads to other members and leads to a disproportionate final collapse status, is responsible for the majority of the most tragic incidents, from the 9/11 event to the Plasco Building collapse. There has been a significant enhancement in our understanding of this phenomenon since the 9/11 event. The main findings are listed and discussed in Kiakojouri et al. (2020a, 2022).

The mainstream code-based progressive collapse analyses predominantly concentrate on a removal strategy for assessing structural robustness. This involves, in static analyses, applying load to the already damaged assembly to perform so-called pushdown analyses, and in dynamic analyses, the sudden removal of a member to examine the subsequent structural response. The damage in this type of study usually entails the removal of one key element, such as a main structural column. The results of such studies have formed the body of our current knowledge, highlighting the effects of initial failure location (Kim and Kim, 2009; Kiakojouri et al., 2020b; Feng et al., 2024) and size (Fu, 2009; Zhang et al., 2020; Yang et al., 2023), building height (Shan et al., 2019; Kiakojouri et al., 2020b), column removal time (Stephen et al., 2019; Kiakojouri et al., 2023a), beam–column connections (Wang et al., 2020; Qiao et al., 2020; Luu and Kim, 2023), and seismic design level (Kordbagh and Mohammadi, 2017; M. Musavi and Sheidaii, 2021). These aspects are primarily related to the availability and strength of alternate load paths.

In parallel, there is an emerging threat-dependent methodology wherein the specific threat is the focal point. The literature in this domain is categorized into blast-, impact-, and fire-induced progressive collapse scenarios. Here, the threat leading to the collapse is directly considered, often resulting in a damage level significantly greater than the single column loss contemplated in code-based methodology. For instance, in a fire scenario, an entire story or multiple stories may be involved, or an explosion may result in the removal of several members along with extensive damage to a large portion of the structure. The emerging literature in threat-dependent discipline has highlighted differences in progressive collapse performance when subjected to specific threats compared to code-based dynamic column removal. These differences, underscored in scenarios involving blast (Ahmed Galal et al., 2020; Kiakojouri et al., 2021), impact (Kang and Kim, 2015; Janfada et al., 2023) and fire (Tavakoli and Kiakojouri, 2015; Gernay and Gamba, 2018; Lan et al., 2023; Guo et al., 2024), are attributed to the number of damaged or removed members and dynamic effects.

Bridging these two methodologies is a specific scenario in which the threat targets a single member, leading to some level of damage to that member, rather than complete failure. At first glance, such cases might appear less critical; however, they warrant attention for

* Corresponding author.
E-mail address: valerio.debiagi@polito.it (V. De Biagi).

https://doi.org/10.1016/j.dibe.2024.100556
Received 29 July 2024; Received in revised form 24 September 2024; Accepted 9 October 2024
Available online 19 October 2024

at least two reasons. Firstly, these scenarios are more common than large-scale damages. This prevalence is due not only to the frequency of smaller threats but also to the robustness of modern structural elements, specially seismically deigned structures, which are unlikely to lose their entire capacity under minor threats. Real-world experiences and experimental research have shown that well-designed structural columns perform remarkably well under extreme loading scenarios, with tearing and full separation being exceedingly rare. Secondly, some studies on structural performance under blast and impact scenarios have indicated that a damaged member can lead to a more critical scenario than a full dynamic removal, emphasizing the importance of focusing on such cases (Kiakojouri et al., 2021; Janfada et al., 2023). Moreover, it should be noted that even if the extreme loading leads to complete failure in a column, the application of damage, while very rapid, is not theoretically *sudden*. This means that during the application of the loads and before the final loss of the column, it can transfer the applied load to the main structure through different mechanisms, predominantly by vertical catenary action.

Analytical tools are used sparingly for assessing progressive collapse in structural frames. These studies are primarily confined to estimating vertical displacement using single and multi-degree of freedom systems with an elastic–plastic compliance law (Biagi et al., 2020). In-depth analytical assessments of collapse-resisting mechanisms are indeed rare, although the concept has been utilized in other fields. Lalkovski and Starossek deeply analyzed the failure propagation mechanism of the Twin Towers thanks to simplified mechanical models, highlighting interesting results on the magnitude of the impact forces generated during pancake-type collapse (Lalkovski and Starossek, 2022). On the contrary, the literature on the collapse of frame elements, say beam or columns is rich and mature. Several studies focused on the damage of single components: for example, numerical analyses on foam-filled circular tubes have shown a better crash ability if compared to other elements (Djamaluddin et al., 2015). Examples of using the simplified sub-structure model for different impact scenarios are reported in Xiang et al. (2024), where simplified methods to predict the robustness of steel parking-structure joints have been proposed.

Considering the aforesaid situations, more focus is needed on structural columns under extreme lateral loading conditions and the involved mechanisms. This paper, for the first time, is exclusively devoted to this phenomenon and highlights the involved catenary mechanism. To serve this aim, both numerical and analytical tools are employed. While the former are applied at the system level, the latter are used for in-depth study of member-level performance. Initially, a series of numerical simulations using a novel IDA-like progressive dynamic method for extreme loading were utilized to clearly demonstrate the structural behavior under blast and impact scenarios. Then, this observation was discussed in depth for using a novel simplified method. The discussed material can provide deeper insights into structural performance under extreme loading scenarios.

2. Numerical examples of phenomenon

Structural response of a steel moment-resisting frame subjected to low-velocity impact and blast scenarios was considered and studied herein to demonstrate the problem in a realistic structural configuration. Several scenarios covering a wide range of impact and blast phenomena were contemplated. Since the numerical analysis of structures under extreme loading conditions is highly dependent on modeling details and adopted finite element techniques, this section is devoted to such aspects. Details of the primary design (Section 2.1), finite element modeling techniques (Section 2.2), dynamic column removal method (Section 2.3), impact loading scenarios (Section 2.4.1), and blast loading scenarios (Section 2.4.2) are provided herein.

2.1. Primary design of the reference structure

The model structure is a four-story steel moment-resisting frame with a floor height of 3.5 meters and beam spans of 5 meters in both directions. Side and plan views of the model structure are illustrated in Fig. 1. The considered dead and live loads are 4.5 and 2 kN/m^2, respectively. All beams and columns are fabricated from St355 steel. Gravity and seismic designs adhered to the Italian building code. Given the location of the structure in Rome (41.89 N; 12.48 E), a Peak Ground Acceleration (PGA) of 0.11 g with a return period of 475 years was used for seismic considerations. The building sits on Soil type C. Box profiles are utilized for columns, while I-sections are employed for beams. The adopted structural sections are listed in Table 1.

2.2. General aspects of finite element modeling

General purpose finite element package Abaqus, was utilized for numerical study. The explicit solver of the software package, which fully accounts for dynamic and nonlinear effects, was employed for both the blast and impact analyses. All beams and columns, except that directly receiving the extreme loads, i.e., Column A in Fig. 1, were modeled by beam element (B31) from Abaqus library. For the blast- and impact-loaded column, a shell type element, i.e., S4R, was used. Being a four-noded reduced integration shell with hourglass control, S4R has been successfully used in blast- and impact-loaded steel structures (Kiakojouri et al., 2021; Janfada et al., 2023). The interactions between beam and shell parts are assured using kinematic coupling.

The significant impact of slabs (Wang et al., 2019; Wang and Wang, 2022; Feng et al., 2022; Yang et al., 2023) and infill walls (Alrubaidi and Alhammadi, 2022a,b; Feng et al., 2022) on the progressive collapse response of frame structures has been highlighted in several recent publications. However, in this study, these effects are deliberately excluded and reserved for future investigation as the purpose of the present work is to understand the fundamental mechanisms that generate in the bare frame. If structural responses of more complex structures are needed, especially for design purposes, these effects must be incorporated in a tailored finite element model that includes the specific geometry and reinforcement arrangement. However, considering that this study emphasizes the comparison of different cases and highlights key mechanisms, the attention is on the frame, only.

In modeling the mechanical behavior of steel material, the nonlinear part is defined as the true stress versus logarithmic strain. While post-yielding behavior is very dominant in cyclic loading conditions, i.e., in seismic analysis, for progressive collapse assessment, especially when the maximum response is the main interest, these effects can be safely simplified or even ignored (Kiakojouri et al., 2020b). Therefore, in this study, a bi-linear elastic–plastic material model was adopted. While strain-rate effects are traditionally ignored for progressive collapse assessment, some recent studies have revealed that they can be important in progressive collapse response, Kiakojouri and Sheidaii (2018), Kiakojouri et al. (2020b). Therefore, strain-rate effects are included in numerical studies using the Cowper–Symonds equation in both progressive collapse and extreme loading analyses. The Cowper–Symonds equation is a well-accepted model for defining the material behavior at high rates (Kiakojouri et al., 2021; Liu and Soares, 2019):

$$\frac{\sigma_{yd}}{\sigma_y} = 1 + \left(\frac{\dot{\varepsilon}}{c}\right)^{\frac{1}{q}}. \tag{1}$$

where σ_{yd} is the dynamic yield stress, σ_y is quasi-static yield stress, c and q are Cowper–Symonds material constants and $\dot{\varepsilon}$ is the strain rate. In the current study $c = 40\ s^{-1}$ and $q = 5$ were adopted, as suggested for progressive collapse assessment of steel frames in Liu and Soares (2019), Kiakojouri et al. (2020b, 2021). Damping ratio of 5% of the critical damping is applied, as usually adopted for analysis of structures undergoing extreme loads (Kiakojouri et al., 2020b). However, the damping impact on maximum response of framed systems in progressive collapse scenarios is negligible and can be safely neglected, as discussed by Kiakojouri and Sheidaii (2018).

Table 1
Cross-sections of structural members for steel frame.

Story	Column ($B \times B \times t$ mm)	Beam ($h \times b_f \times t_f \times t_w$ mm)		
		NLB	Perimeter-LB	Internal-LB
1	250 × 250 × 16	330 × 160 × 11.5 × 7.5	360 × 170 × 12.7 × 8	400 × 180 × 13.5 × 8.6
2	250 × 250 × 16	330 × 160 × 11.5 × 7.5	360 × 170 × 12.7 × 8	400 × 180 × 13.5 × 8.6
3	250 × 250 × 8	330 × 160 × 11.5 × 7.5	360 × 170 × 12.7 × 8	400 × 180 × 13.5 × 8.6
4	250 × 250 × 8	330 × 160 × 11.5 × 7.5	360 × 170 × 12.7 × 8	400 × 180 × 13.5 × 8.6

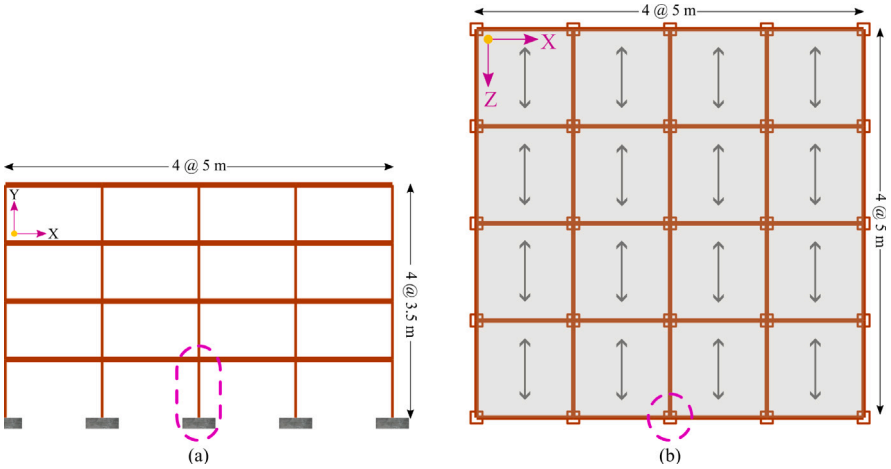

Fig. 1. Model structure and the initial failure case; (a) side view and (b) plan view.

2.3. Dynamic column removal scenario

Dynamic column removal analysis was performed to provide a basis for comparison of impact- and blast-loaded frames with the code-based threat-independent (TI) approach. For dynamic column removal, Initially, gravity loads were statically applied on the intact structural assembly. A load combination of $1.2DL + 0.5LL$ (DL and LL stand for dead load and live load, respectively) is adopted. Then, *"*model change, remove"* command from Abaqus library is utilized for abrupt column removal. Column removal case, that is similar to that accepting the blast and impact loads, is shown in Fig. 1. Such a methodology is widely adopted in threat-independent progressive collapse studies of frame systems (Kiakojouri et al., 2020b). Otherwise, more time-consuming approaches, i.e., so-called force-based column removal approach (Kim and Kim, 2009), or other innovative methods, i.e., degradation method (Tavakoli and Kiakojouri, 2013), should be utilized. Column removal time, i.e., t_r is considered as 0.001 s, and 1 s monitoring period after removal is adopted, the rationale is discussed in Kiakojouri et al. (2023a), GSA (2013), Kiakojouri and Sheidaii (2018). Based on the methodology described above, the vertical displacement at the column removal point is observed to be 33.4 mm. This value is used in subsequent sections for comparison between the threat-independent code-based column removal method and threat-dependent blast and impact analyses.

2.4. Impact and blast loading scenarios

Two classes of extreme loading cases to address the blast and impact scenarios are considered. Details of each scenario and the adopted parameters are described in the subsequent subsections for impact (2.4.1) and blast (2.4.2). The extreme loading scenarios are applied to Column A as described in Fig. 1. Inspired by incremental dynamic analysis (IDA) (Vamvatsikos and Cornell, 2002), an incremental approach to extreme loading is utilized. In this novel approach, the intensity of extreme loading is increased in several steps, and each time the maximum response, i.e., the maximum vertical displacement at the column top node, is computed. To achieve this, in blast analyses the charge weight is incrementally increased for different standoff distances, and the maximum response is computed. Similarly, in impact analyses, the weight of the impactor is increased each time, and the maximum displacement is recorded for each cycle for different velocity. These maximum responses are then used to draw a new curve, the so-called dynamic pushdown curve, which illustrates the maximum responses versus different extreme loading scenarios. This methodology provides more insight compared to traditional time–history curves, as it highlights structural performance under various load levels. The maximum response from code-based dynamic column removal can also be used for comparison. Fig. 2 shows an example of the incremental methodology adopted for blast and impact analyses.

Before the application of the extreme scenarios, i.e., blast and impact loading, the vertical gravitational load was applied to the frame assembly. Obviously, the load combination for extreme loading scenarios is similar to what is described for dynamic column removal, i.e., $1.2DL+0.5LL$. Since the entire analysis occurs in a single dynamic step, and to avoid unwanted dynamic effects in an inherently quasi-static loading condition, i.e., gravitational service load, the load was gradually increased over 0.5 s, then maintained unchanged for another 0.5 s. The extreme loading was applied at t=1 s, and the structural response was monitored for an additional 0.5 s, which proved to be sufficient for the development of the maximum response.

It should be noted that several simplifications and assumptions are applied when modeling extreme scenarios. While these simplifications limit the application of the current methodology for the design and analysis of real structures, they serve the primary colorblackaim of this study. For instance, façades and infill walls, which are not considered here, may offer some resistance to blast loads and, in some cases, transfer loads to connecting columns. Additionally, connection behavior is not included; in a real blast or impact scenario, failure may occur at the connections, which cannot be predicted in this simplified model. However, these issues do not affect the key concept being demonstrated. In a model tailored to include the effect of a specific infill, the illustrated behavior could appear in a shifted load range, with the floor system and infill walls contributing to vertical catenary forces and non-structural elements engaging in energy dissipation, especially at larger displacements. These secondary mechanisms, although excluded to clarify the

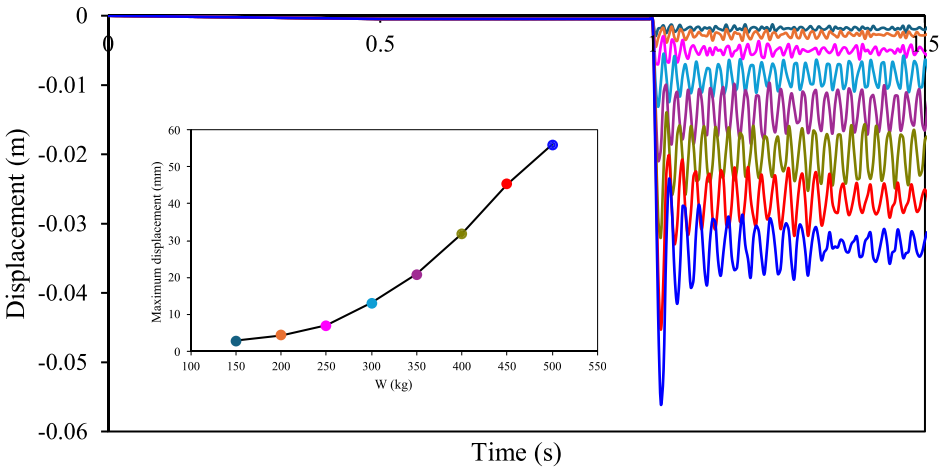

Fig. 2. An example of time–history analyses performed to develop the Impact/Blast Incremental Dynamic Analysis (I-IDA or B-IDA) curve. The IDA curve is shown in the inset.

basic behavior in this study, remain important considerations in real structural systems and leave open questions regarding their roles in resisting such forces.

To consider a reasonable range of possible threats, for both impact and blast scenarios, three classes (velocities for impact and standoff distances for blast) are considered. Subsequently, the other influencing parameter (impactor weight for impact and explosive charge weight for blast) is incrementally increased across eight levels, resulting in 48 extreme loading scenarios. Among these, eight scenarios (four for blast and four for impact analyses) are ultimately excluded from further investigation, either due to the insufficiency of the utilized numerical techniques or due to very low or very high displacements. This results in 20 scenarios each for impact and blast being implemented. The specific details of numerical techniques are demonstrated in the following subsections.

2.4.1. Impact scenarios

Several impact scenarios were defined to cover a reasonable range of mass and velocity. As discussed in Section 1, some previous studies have focused on threat-related impact scenarios, i.e., consideration of the details of the possible impactor, namely a truck, with different levels of simplifications. However, here, a simplified approach is preferred. It is because the current study is not devoted to any specific threat, instead, in a more general framework, the structural response of the impact-loaded frame is monitored. Simplified general impact scenarios, i.e., simple geometry varying in mass and velocity can serve this aim successfully. For case studies and design purposes, an advanced, detailed model tailored to the specific threat, structural exposure, and importance must be developed, accounting for deformation and energy dissipation in the impactor, which may influence the structural response. A detailed finite element model or an equivalent approach should be used for this purpose. However, as this paper focuses on highlighting basic mechanisms and drawing comparisons, rather than precise modeling of the impact scenario, such aspects are beyond its scope.

In this study, three velocities, i.e., 10, 20, and 30 m/s, are considered. For each velocity, an IDA-like analysis is performed by increasing the impactor's mass from 500 to 4000 kg. Fig. 3 shows the overall configuration, loading sequence, and adopted impact scenarios. While there is no special emphasis on a realistic threat modeling, the selected scenarios are in the range of the normal vehicle (Song et al., 2021) and/or rockfall (De Biagi et al., 2020) impacts and can be considered as representative of these phenomena. The impactor is modeled as a rigid body with the height of 0.25 m and the length of 0.5 m. The impact point is considered in mid-height of the selected column.

2.4.2. Blast scenarios

The threat posed by a conventional bomb can be characterized by two fundamental parameters: the explosive charge weight and the standoff distance. The blast pressure time–history is divided into two phases: a positive phase and a negative phase. During the positive phase, the maximum over-pressure, P_s^+, increases rapidly and then decreases to ambient pressure, P_0, within the duration T^+. Conversely, in the negative phase, the maximum negative pressure, P_s^-, has a lower amplitude and a longer duration (T^-) compared to the positive phase. Therefore, it is recommended that numerical studies of blast-loaded structures primarily focus on the positive phase. The pressure time–history can be approximated by the following exponential equation (Eq. (2)):

$$P(t) = P_s^+ \left(1 - \frac{t}{T^+}\right) e^{\frac{-bt}{T^+}}. \tag{2}$$

where $P(t)$ is overpressure at time t, P_s^+ is maximum over pressure and b is experimental constant.

Abaqus/Explicit integrates the ConWep model, which is specifically developed for simulating air blast loading on structures. This model calculates scaled distances from target surfaces to the explosion source and utilizes the equivalent weight (Xiao et al., 2020) of Trinitrotoluene (TNT) to determine the explosive charge amount. In ConWep, the total pressure exerted on a surface by the blast wave is determined by the incident pressure, the reflected pressure, and the angle of incidence. The total pressure is mathematically expressed as shown in Eq. (3):

$$P(t) = P_{incident}(t)\left[1 + \cos(\theta) - 2\cos^2(\theta)\right] + P_{reflect}(t)\cos^2(\theta) \tag{3}$$

where $P(t)$ is total pressure, $P_{incident}(t)$ and $P_{reflect}(t)$ are incident pressure and reflected pressure respectively, and θ is angle between the normal of the loading surface and the vector that points from the surface to the blast source.

In this study, the aforementioned incremental methodology was applied to three standoff distances: 1, 1.5, and 2 m. Analyses were repeated with explosive weights ranging from 150 kg to 500 kg. For each subsequent case, the weight was increased by 50 kg, and the maximum response was calculated, resulting in a total of eight analyses for each standoff distance. Fig. 4 shows the details of blast analyses and adopted scenarios. Among the considered cases, four were eliminated because, according to previous studies, they do not fall within the desirable range of blast loading for the adopted numerical technique (Forni et al., 2017; Kiakojouri et al., 2021).

3. Numerical results and discussions

The results of impact and blast analyses are summarized in Figs. 5 and 6, respectively. In these figures, the dashed red line represents

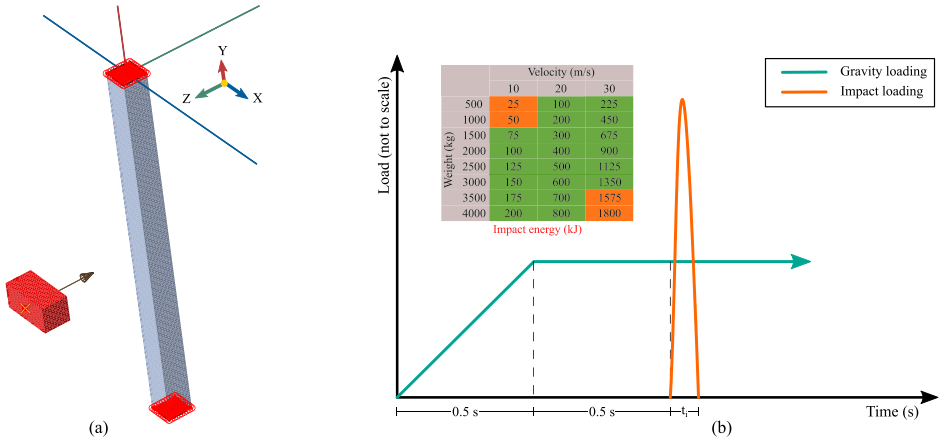

Fig. 3. Numerical modeling of the impact-loaded model structure: (a) general configuration in finite element modeling and (b) loading sequence and adopted impact scenarios. (For interpretation of the references to color in this figure legend, the reader is referred to the web version of this article.)

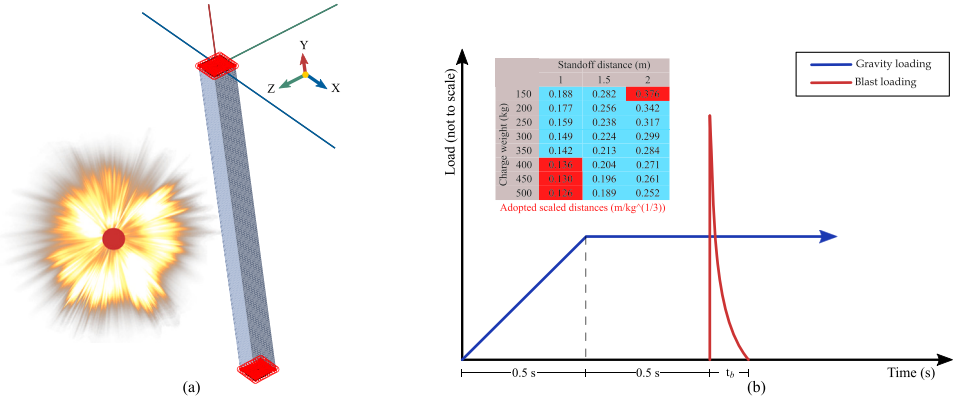

Fig. 4. Numerical modeling of the blast-loaded model structure: (a) general configuration in finite element modeling and (b) loading sequence and adopted blast scenarios. (For interpretation of the references to color in this figure legend, the reader is referred to the web version of this article.)

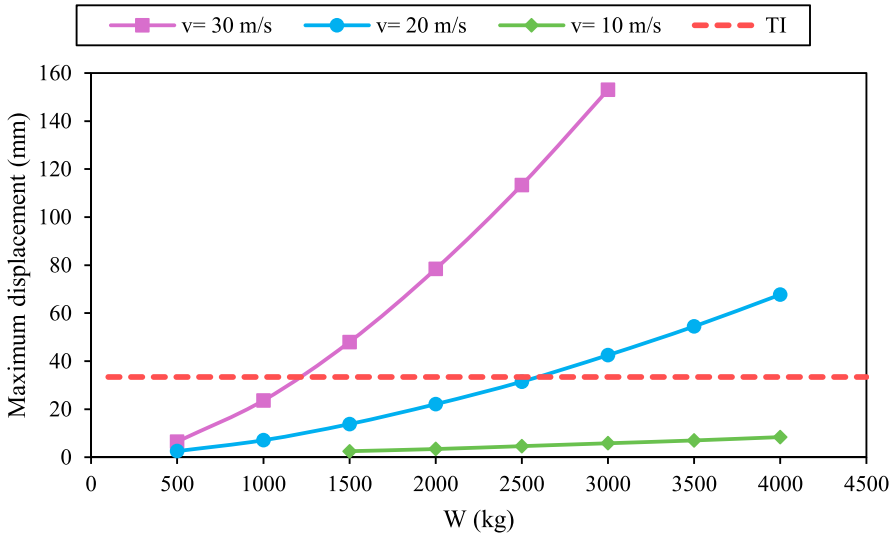

Fig. 5. I-IDA curves for three different velocities. Maximum vertical displacement in TI dynamic column removal analysis is shown for comparison.

the maximum vertical displacement in code-based, threat-independent column removal, based on the methodology described in Section 2.3. It is immediately evident that the structural response, i.e., vertical displacement in top node of damaged column, can exceed the equivalent displacement in dynamic column removal analysis in many cases.

Fig. 5 demonstrates the maximum response for 20 impact scenarios as introduced in Fig. 3. While the maximum responses for all cases at a velocity of 10 m/s are significantly lower than those seen in dynamic column removal, for the other two cases, i.e., velocities of 20 m/s and 30 m/s, the responses exceed the code-based displacement beyond a

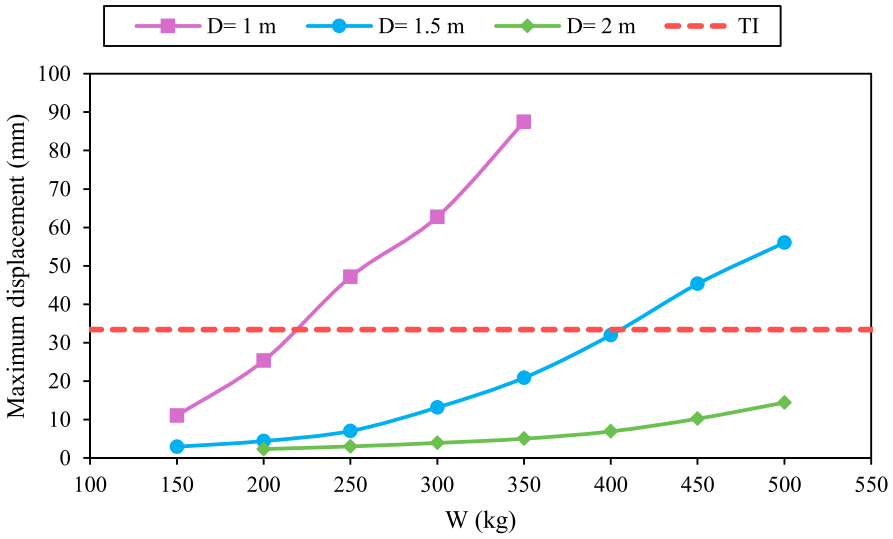

Fig. 6. B-IDA curves for three different standoff distances. Maximum vertical displacement in TI dynamic column removal analysis is shown for comparison.

certain level. For instance, in the most critical scenarios at velocities of 30 m/s (3000 kg) and 20 m/s (4000 kg), the maximum responses increase by 458% and 202%, respectively. The results also highlight the much greater influence of velocity compared to mass in affecting dynamic response, a prediction that aligns with the basic principles of the kinetic energy equation.

Fig. 6 illustrates the maximum response for 20 blast scenarios as introduced in Fig. 4. For the standoff distance of 2 m, the maximum response for all charge weights remains lower than the dynamic column removal estimation. Conversely, for the other two standoff distances, namely 1 and 1.5 m, the maximum response significantly exceeds the threat-independent dynamic column removal response after a certain charge weight. In the most critical cases, the maximum response reached 262% and 168% of the TI column removal response for charges of 350 kg at 1 meter and 500 kg at 1.5 m, respectively. The results also highlight the greater influence of standoff distance compared to explosive charge, underscoring the importance of nonstructural protection measures.

It should be underlined that in all the considered cases, no removal occurred, and the column remained connected to the structure with a certain level of damage after the event. However, as detailed, the response can easily exceed that of sudden and complete column removal. This observation can be attributed to the development of a catenary force in the laterally loaded column. The still-connected column can transfer this load into the main system, leading to greater vertical downward displacement even compared to sudden column loss. In Section 4, a simplified column model is presented to assess the catenary effects during impact scenarios, which may further elucidate the numerical observations.

4. A simplified column model to assess the catenary effects during impact

A simple analytical model is proposed to highlight the mutual effects that occur in a loaded column subjected to lateral impact. The studied element is part of a larger frame structure and it is supposed to be the support of the first floor. Hence, its bottom end is fixed in the ground, while its top end is connected to the frame. The single-column component, shown in Fig. 7.a, is fully constrained at its ends. The column is subjected to an axial force U due to the weight of the stories above. In the model, the axial force is considered as an initial pre-constrain stress. For sake of simplicity, the stiffness of the remaining frame structure is not considered in the model. vertical stiffness k_1 is the result of the elastic vertical contribution of the structure. The column is subjected to an impact force F acting at its mid-height and resulting from the external action.

A horizontal force F acting at mid-height causes a symmetrical bending moment distribution with top and bottom bending moments equal to $Fh/8$ (left-hand column side is in traction) and a mid-height bending moment of $Fh/8$ (right-hand column side is in traction). The structural element undergoes plastic deformations when subjected to the impact force. This analysis is performed with the generalized variables approach proposed in the literature (Chen et al., 2007). Instead of considering the stresses in each point of the element, the approach considers as generalized stresses the resultant forces such as the bending moment or the axial force. Similarly, the generalized strains are the elongation of the column and the rotation in the plastic hinges. The relation between generalized stresses and generalized strains is expressed by the yield criterion, as illustrated in the following. The maximum force that the system is able to support in its elastic regime depends on the magnitude of the axial compression force U. Based on the magnitude of U, the plastic bending moment is defined. We recall as F_p the force that causes the formation of the plastic hinge. Under a suitable approximation, the lateral displacement at yielding, δ_p, derives from the flexural theory of elastic beams and it is equal to:

$$\delta_p = \frac{F_p h^3}{192EI}, \tag{4}$$

where I is the inertia of the cross-section around the out-of-plane axis.

At F_p, plastic hinges form at both ends of the column and at its midspan, i.e. at points A, B and C of Fig. 7.b. A larger value of F causes plastic deformations: plastic rotations and plastic elongations occur at plastic hinges. Recalling δ the lateral displacement at mid-height, the total elongation Δ of the column can be written as:

$$\Delta \approx \frac{2\delta^2}{h}, \tag{5}$$

being the sum of elastic and plastic components, Δ_{el} and Δ_{pl} respectively. Hence, the elastic elongation is:

$$\Delta_{el} = \Delta - \Delta_{pl} = \frac{2\delta^2}{h} - \Delta_{pl}. \tag{6}$$

Considering that the column has an axial stiffness equal to:

$$k_{ax} = \frac{EA}{h}, \tag{7}$$

where A is the cross-section area, the axial force in the column is the product of the elastic elongation times the axial stiffness, plus the initial axial force:

$$N = k_{ax}\left[\frac{2\delta^2}{h} - \Delta_{pl}\right] + U, \tag{8}$$

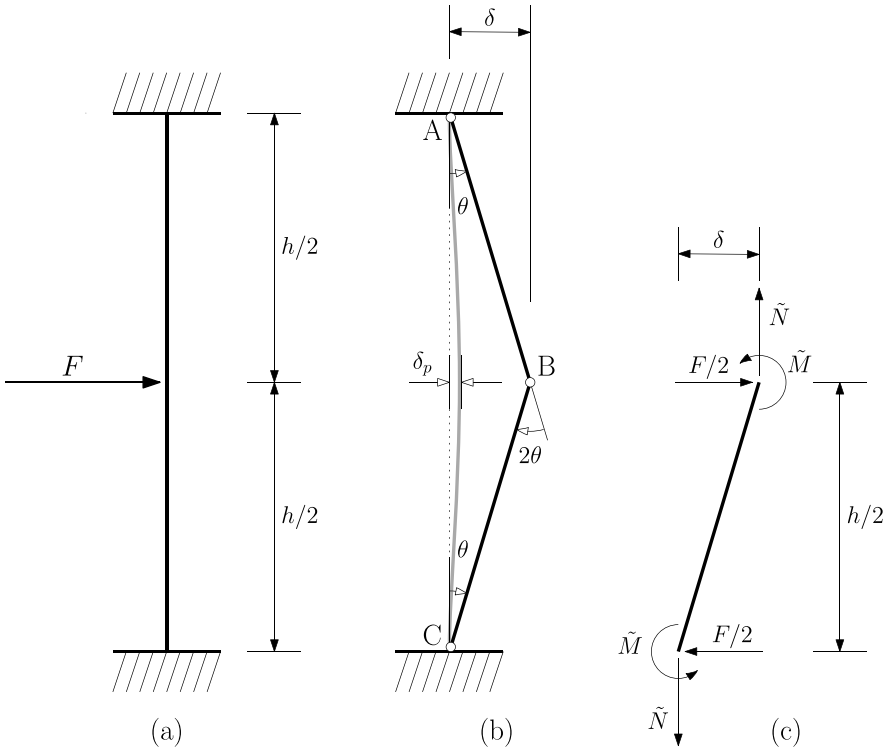

Fig. 7. Sketches of the impacted column: (a) physical model of the column with both ends fixed; (b) displacements following the formation of the plastic hinges, refer to the text for the details; (c) forces acting on half column.

The plastic elongation occurs when the cross-section of the beams experience plasticity. The yield function, which defines the elastic limit for any possible combination of generalized stresses, can we written as:

$$f = \omega \left(\frac{M}{M_u}\right) \pm \gamma \left(\frac{N}{N_u}\right)^{\alpha} - 1 = 0, \tag{9}$$

where ω, γ and α are three parameters that describe the shape of the yield surface for complex cross-section shapes, M_u and N_u are the ultimate bending and axial force, respectively. The $\pm$ in Eq. (9) considers either traction (+) and compression (−) axial forces. The generalized strains rates are the sum of elastic and plastic strain rates. The latter are derived from a plastic potential: in the case of associated flow rule, the plastic strain rate vector is normal to the yield surface, resulting in:

$$\begin{pmatrix} d\theta_{pl} \\ d\Delta_{pl} \end{pmatrix} = \mu \begin{pmatrix} \partial f/\partial M \\ \partial f/\partial N \end{pmatrix}, \tag{10}$$

where θ_{pl} is the plastic rotation in the plastic hinges and μ is a positive factor of proportionality.

Eq. (8) can be derived with respect to the lateral displacement δ, resulting in:

$$\frac{dN}{d\delta} = k_{ax}\left[\frac{4\delta}{h} - \frac{d\Delta_{pl}}{d\theta_{pl}}\frac{d\theta_{pl}}{d\delta}\right], \tag{11}$$

where θ_{pl} is the rotation at the plastic hinges. The derivative $d\theta_{pl}/d\delta$ is the amount of total rotation at the plastic hinges during the mechanism: with the assumption of small displacements, it can be rewritten as $8/h$. The derivative $d\Delta_{pl}/d\theta_{pl}$ can be obtained from Eq. (10) by removing the factor of proportionality, resulting in:

$$\frac{d\Delta_{pl}}{d\theta_{pl}} = \frac{\partial f/\partial N}{\partial f/\partial M}. \tag{12}$$

Hence, Eq. (11) can be rewritten as:

$$\frac{dN}{d\delta} = k_{ax}\left[\frac{4\delta}{h} - \frac{\partial f/\partial N}{\partial f/\partial M}\frac{8}{h}\right] \tag{13}$$

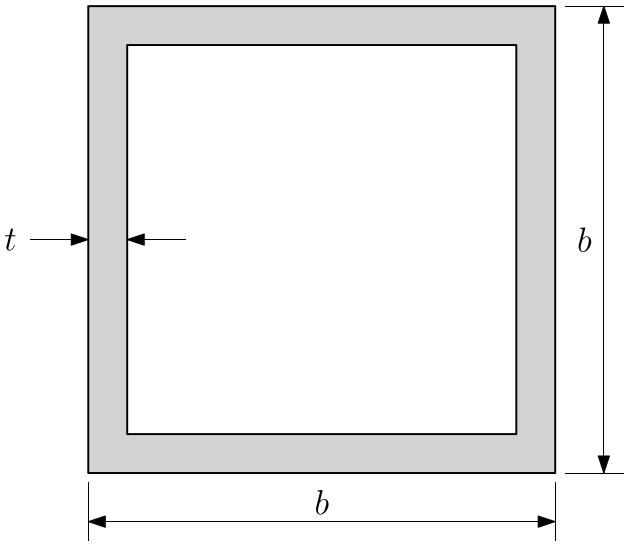

Fig. 8. Geometry of the square hollow cross-section.

and integrated along the displacement δ with a step-by-step procedure, starting from the transition between elastic to plastic behavior at $\delta = \delta_y$ for which $N = U$. To account for the non uniqueness of the yield function, the limitation $|N| \leq |N_u|$ must be imposed. For a given $\tilde{N} = N(\delta)$, the corresponding bending moment $\tilde{M} = M(\delta)$ satisfying the yield function of Eq. (9) is determined. From the equilibrium of half column, see Fig. 7, the force $F(\delta)$ is computed as:

$$F(\delta) = \frac{4}{h}\left(\tilde{N}\delta - 2\tilde{M}\right). \tag{14}$$

With reference to the examples discussed in Section 2, the considered column has a rectangular hollow cross-section, as depicted in

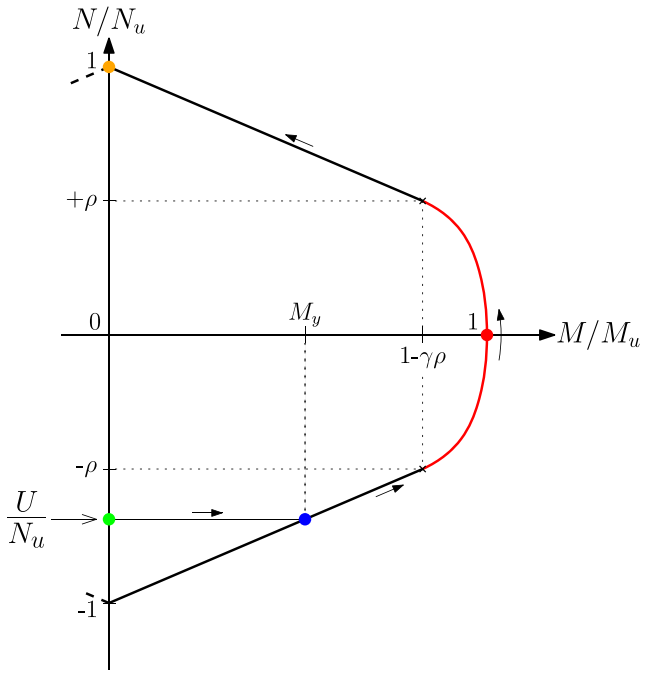

Fig. 9. Bending moment - Axial force yield function. The dots refer to specific conditions, as reported in the text.

Fig. 8, and it is made of elastic-perfectly plastic material having Young Modulus E and yield strength f_y. Neglecting the possibility of buckling, previous studies (Yin and Wang, 2005) identified the yield function between bending moment M and axial force N based on the position of the neutral axis in the cross-section. If the neutral axis is in the web, the parameters of the flow rule of Eq. (9) are:

$$\begin{cases} \omega = 0 \\ \gamma = \frac{(1+\beta)^2}{\beta(4+\beta)} \\ \alpha = 2 \end{cases} \tag{15}$$

with $\beta = \frac{b-2t}{b}$. If the neutral axis is in the flanges, the parameters of the flow rule of Eq. (9) are:

$$\begin{cases} \omega = \omega = \frac{1-\rho}{1-\gamma\rho^2} \\ \gamma = 0 \\ \alpha = 1 \end{cases} \tag{16}$$

with

$$\rho = \frac{b-t}{2b-t}. \tag{17}$$

The ultimate bending and axial force, M_u and N_u are computed as the product of the plastic modulus or the cross-section times the yield stress, respectively. The transition between web – Eq. (15) – and flanges – Eq. (16) – regime occurs at $M/M_u = 1 - \gamma\rho^2$ and $N/N_u = \pm\rho$.

Fig. 9 depicts the yield interaction diagram between axial force and bending moment. The red curve refers to the case in which the neutral axis is in the web, hence the parameters of Eq. (15) holds; the black straight lines relate to bending-axial force interaction when the neutral axis is in the flange, according to the parameters of Eq. (16).

When no horizontal force is applied, only an axial compression force U acts on the column, corresponding to the greed bullet in Fig. 9. The initial yielding occurs when the bending moment due to F, coupled with the axial force U, let the f to zero, i.e. the blue bullet in Fig. 9. Hence, it does not usually result $M_y = M_u$.

4.1. Model validation

Fig. 10 depicts the values of the force F with respect to the lateral displacement δ for a 3.5 m tall, $250 \times 250 \times 16$ mm - St355 hollow square column subjected either to no axial load, i.e. $U = 0$ kN, or to a compression axial load of $U = -1000$ kN. A elastic-perfectly plastic material model was adopted. The analysis was performed analytically (black curves) and numerically (red curves). The latter has been obtained considering an elastic-perfectly plastic material behavior, a force applied at mid-height over a rectangular area of 250×250 mm^2; the displacement is measured in the mid-height side face of the column. A good agreement between the curves is observed. The simplifications introduced in the model emerge in the comparison. The numerical model catches the formation of the plastic hinge and the transition from elastic-to-plastic behavior; on the contrary, the analytical model considers that the elastic stage ends when the plastic hinge is completely formed. Despite the simplification, the magnitude of the force is similar in both models. The analytical model catches the transition between flexural and catenary behaviors, that rises at a displacement of 0.2 m, approximately, with a change in the slope of the force–displacement curve.

4.2. Catenary force during impact and effects on the structure

Fig. 11 depicts the value of the force F with respect to the lateral displacement δ and the interaction plot for a 3.5 m tall, $250\times250\times16-St355$ hollow square column subjected to an initial axial compression force of 420 kN. It is seen that following the elastic regime (linear ramp up to the blue dot), a stiff hardening occurs up to the red dot as the yield bending moment increases following a reduction of the compressive axial force. Following this point, a softer hardening is observed up to the orange dot representing the transition between bending and catenary resisting mechanisms.

During the threat, the kinetic energy to be absorbed by the impacted column is:

$$K = \frac{1}{2} m_i v^2, \tag{18}$$

where m_i is the mass of the striking body and v its velocity. The energy demand, namely $\mathcal{K}$, accounts for the mass of the column that is activated during the plastic mechanism, i.e. the effective mass m_c^e, and the striking mass. Considering the three hinges mechanism that forms, m_c^e is half the total mass of the column (Ventura et al., 2017). Under the hypothesis that the striking body rebounds, which happens if the impacted member has a non-negligible mass, the resulting energy demand is Yong et al. (2022):

$$\mathcal{K} = K\lambda \left(\frac{1 + \mathrm{CoR}}{1 + \lambda} \right)^2, \tag{19}$$

where $\lambda = m_c^e/m_i$. The coefficient of restitution CoR considers the contact energy dissipation and depends on material types.

The integral of $F - \delta$ curve can be interpreted as the energy dissipated by the column, $\mathcal{D}$. For a given displacement $\delta°$, it results:

$$\mathcal{D}\left(\delta^\circ\right) = \int_0^{\delta^\circ} F\left(\delta\right) d\delta, \tag{20}$$

which is a monotonically increasing function. Thus, it can be inverted and the relationship between energy and displacement can be determined. By equating energy demand and dissipated energy, i.e. $\mathcal{K} = \mathcal{D}$, the maximum displacement is first computed and the corresponding axial force is determined. If the axial force is larger zero, a detrimental vertical catenary force is transferred to the structure through the top end of the column, causing an additional downward displacement of the structure.

Fig. 12 reports the results of a parametric analysis to quantify the influence of the impacting mass and velocity on the expected axial force in the column due to catenary forces that raise during the interaction.

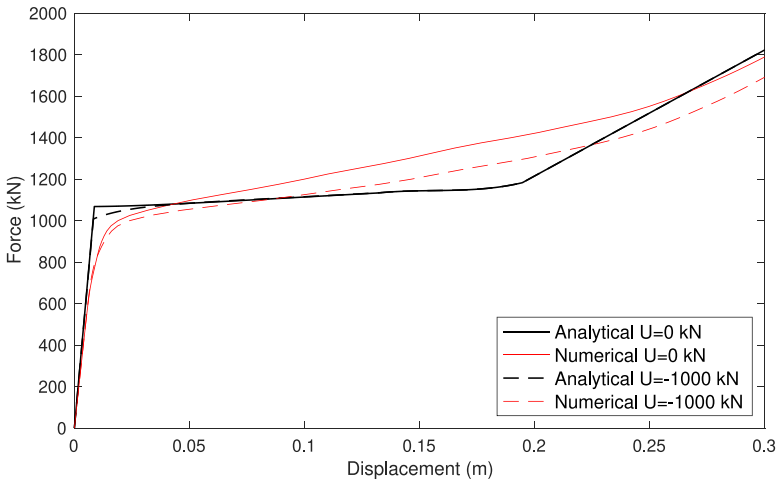

Fig. 10. Force F *vs* lateral displacement δ validation curve for a 3.5 m tall, $250 \times 250 \times 16 - St355$ hollow square column. The black curves refer to the results of the analytical model, the red curves to the results of the FEM analysis. Two different initial axial forces are considered. (For interpretation of the references to color in this figure legend, the reader is referred to the web version of this article.)

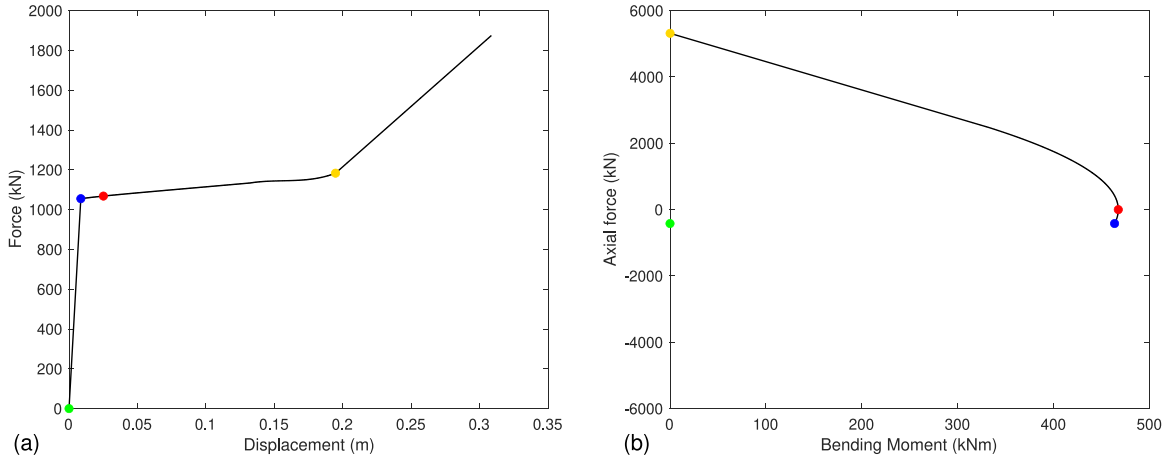

Fig. 11. Force F *vs* lateral displacement δ curve and interaction diagram for a 3.5 m tall, $250 \times 250 \times 16 - St355$ hollow square column subjected to an axial compressive force of −420 kN.

The initial axial force is set to −420 kN and the impacting mass m_i ranges between 50 and 2000 kg. Three velocities are considered: 10, 20 and 30 m/s. The total mass of the column is equal to 411.5 kg, while the effective mass in the calculations is equal to $m_c^e = 206$ kg. The coefficient of restitution (CoR) is set to 0.3, as reported in the literature for steel-concrete impacts (Yong et al., 2022, 2020). It is shown that for impact velocities equal to 10 m/s, the column is still compressed independently from the size of the impacting mass, meaning that it is still able to support the above structure. For larger velocities, the column experiences tensile axial forces: for an impact velocity of 20 m/s, tension is expected for masses larger than 260 kg, while for an impact velocity of 30 m/s the figure drops to 125 kg.

Comparing the actual results with the current practice resulting from threat-independent damage scenarios, i.e. the sudden removal of the column with consequent dynamic effects on the structure due to abrupt lack of support, it can be stated that the additional downward force acting on the structure due to the catenary forces that originates in the column constitutes a threat to frames.

5. Conclusions and future research directions

To verify the application of the alternate load path method in progressive collapse assessment, and understand its limitations, it is crucial to focus more on a threat-dependent methodology. The current study is devoted to this purpose, concentrating on the parameters affecting the dynamic response and load-transferring mechanisms of an impact- and blast-loaded steel moment-resisting frame. The differences in structural responses between the threat-independent method, i.e., dynamic column removal, and the threat-dependent method, i.e., impact and blast analyses, are highlighted. Finally, a simple yet robust analytical model describing the behavior of an impact-loaded column is developed.

It should be noted that the results are obtained for a regular steel frame, where the damage is concentrated in a single column and the predominant collapse mechanism is redistribution-type. These results should be interpreted within this specific domain only. Furthermore, the findings are valid only within a specific range of extreme scenarios and are not necessarily extendable to other cases.

As reviewed, the velocity of the impactor in a impact scenario and standoff distance in a blast scenario are among the most important variables that governs the system's dynamics. Development and application of the non-structural measures, that can stop the impactor or decrease its velocity efficiently, or decrease the intensity of an external explosion are of great importance to control the initial damage size and intensity.

The comparison of threat-independent and threat-dependent results underscores that the response in a structure with a damaged column can far exceed the equivalent response when the column is fully and suddenly removed. This observation explains why the vertical displacement at the column's top node in blast and impact scenarios can exceed

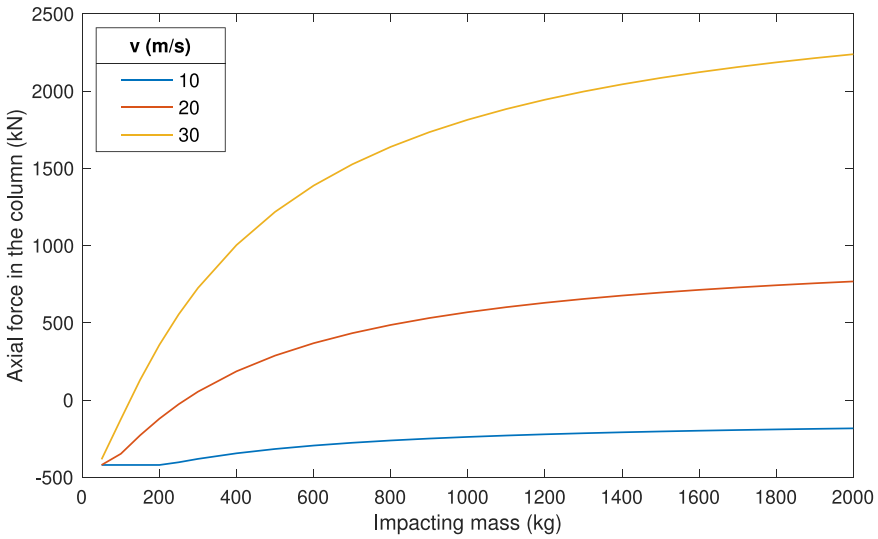

Fig. 12. Axial force in the column due to the catenary forces that generate during the impact. Various masses and impact velocities are considered in the analysis. (For interpretation of the references to color in this figure legend, the reader is referred to the web version of this article.)

the dynamic column removal response, even while the column remains connected to the system and retains residual capacity. These findings are of great importance for progressive collapse analyses. In mainstream research methodology and also in progressive collapse design guidelines, column removal is suggested for initial failure modeling and is usually considered a simple yet conservative and safe choice compared to more realistic damage modeling. The current findings underscore that the opposite situation is possible too.

The obtained results also underline the importance of concepts like passive (Makoond et al., 2024) and active compartmentalization (Kiakojouri et al., 2023b). In these concepts, a preinstalled fuse-like element in the structural assembly prevents the transfer of extreme loads to other structural members, thereby controlling collapse propagation. These concepts have recently been materialized for threat-independent progressive collapse, i.e., dynamic column removal, but the current results highlight the need for similar technology for extreme loading conditions as well.

To further highlight and explain the numerical observations, a simple but robust analytical framework was developed, demonstrating good agreement between the analytical and numerical findings. The developed model not only efficiently describes the interaction between axial and lateral mechanisms and assesses the catenary effect when a structural column is subjected to lateral impact loading, but it can also technically serve as a basis for several similar cases. Future analytical studies will include hardening in the material model and account for the contribution of the surrounding structure, not included in the present model.

As the first study exclusively focused on this phenomenon, emphasis is placed on basic mechanisms, with several simplifications and assumptions adopted in the methodology. For example, the effects of infill walls and the possible influence of non-structural elements are not considered. The effects of infill walls on the progressive collapse response are well-established. As highlighted in seismic engineering, non-structural elements can contribute to resistance mechanisms and modify load paths. Therefore, these elements could contribute to collapse resistance through secondary mechanisms. While the basic phenomenon is clearly explained using numerical examples and fundamental mechanisms highlighted through an analytical approach, there remains room for more detailed models to address real collapse incidents with greater accuracy.

This study delves into the development of catenary effects during impact scenarios and highlights the effect of such a mechanism on the progressive collapse response of multi-story, multi-span frame systems. The proposed analytical methodology elucidates the involved mechanisms during an impact or small near-field explosion when extreme loading is applied to a limited area on the column face. However, similar catenary action is also anticipated in other extreme events, even when the lateral load is more or less uniformly distributed across the full height of the columns, as can occur in a far-field explosion or debris flow. In such cases, an update to the proposed formulation is needed to fully explain the phenomenon, which is reserved for future research. Finally, it should be noted that the current methodology in this study is applied to steel structures. However, it is anticipated that similar behavior can also be observed in other construction materials, notably reinforced concrete structures. Applying such analyses to reinforced concrete members and addressing their unique challenges can be considered in future research. The findings are, obviously, relevant in other structural configurations where impact or blasts are expected.

CRediT authorship contribution statement

Foad Kiakojouri: Writing – review & editing, Writing – original draft, Methodology, Formal analysis, Conceptualization. **Valerio De Biagi:** Writing – review & editing, Writing – original draft, Methodology, Formal analysis, Conceptualization.

Declaration of competing interest

The authors declare that they have no known competing financial interests or personal relationships that could have appeared to influence the work reported in this paper.

Acknowledgments

This paper was partially carried out within the RETURN Extended Partnership and received funding from the European Union Next-GenerationEU (National Recovery and Resilience Plan – NRRP, Mission 4, Component 2, Investment 1.3 – D.D. 1243 2/8/2022, PE0000005).

Data availability

Data will be made available on request.

References

Ahmed Galal, M., Bandyopadhyay, M., Krishna Banik, A., 2020. Progressive collapse analysis of three-dimensional steel–concrete composite building due to extreme blast load. J. Perform. Constr. Facil. 34, 04020021.

Alrubaidi, M., Alhammadi, S., 2022a. Investigation of different infill wall effects on performance of steel frames with shear beam–column connections under progressive collapse. Lat. Am. J. Solids Struct. 19, e432.

Alrubaidi, M., Alhammadi, S., 2022b. Effectiveness of masonry infill walls on steel frames with different beam–column connections under progressive collapse. Structures 38, 202–224.

Biagi, V.D., Kiakojouri, F., Chiaia, B., Sheidaii, M.R., 2020. A simplified method for assessing the response of rc frame structures to sudden column removal. Appl. Sci. 10, 3081.

Chen, W.-F., Han, D.-J., Han, D.-J., 2007. Plasticity for Structural Engineers. J. Ross publishing.

De Biagi, V., Marchelli, M., Peila, D., 2020. Reliability analysis and partial safety factors approach for rockfall protection structures. Eng. Struct. 213, 110553.

Djamaluddin, F., Abdullah, S., Ariffin, A., Nopiah, Z., 2015. Non-linear finite element analysis of bitubal circular tubes for progressive and bending collapses. Int. J. Mech. Sci. 99, 228–236.

Feng, F.-F., Hwang, H.-J., Zhou, Y., Sun, J.-M., Zhang, H.-Z., Roh, J.-H., Kang, S.-M., Yi, W.-J., 2024. Effect of three-dimensional space on progressive collapse resistance of reinforced concrete frames under various column removal scenarios. J. Build. Eng. 90, 109405.

Feng, D.-C., Zhang, M.-X., Brunesi, E., Parisi, F., Yu, J., Zhou, Z., 2022. Investigation of 3d effects on dynamic progressive collapse resistance of rc structures considering slabs and infill walls. J. Build. Eng. 54, 104421.

Forni, D., Chiaia, B., Cadoni, E., 2017. Blast effects on steel columns under fire conditions. J. Constr. Steel Res. 136, 1–10.

Fu, F., 2009. Progressive collapse analysis of high-rise building with 3-d finite element modeling method. J. Constr. Steel Res. 65, 1269–1278.

Gernay, T., Gamba, A., 2018. Progressive collapse triggered by fire induced column loss: Detrimental effect of thermal forces. Eng. Struct. 172, 483–496.

GSA, 2013. Alternate path analysis & design guidelines for progressive collapse resistance.

Guo, Z., Yang, K., Xing, Z., Nie, Z., Chen, Y., 2024. Experimental and numerical study on extended endplate beam–column joints after high temperature to resist progressive collapse. J. Constr. Steel Res. 219, 108795.

Janfada, I.S., Sheidaii, M.R., Kiakojouri, F., 2023. Comparative analysis of code-based dynamic column removal and impact-induced progressive collapse in steel moment-resisting frames. Int. J. Steel Struct. 23, 1576–1586.

Kang, H., Kim, J., 2015. Progressive collapse of steel moment frames subjected to vehicle impact. J. Perform. Constr. Facil. 29, 04014172.

Kiakojouri, F., De Biagi, V., Abbracciavento, L., 2023b. Design for robustness: Bio-inspired perspectives in structural engineering. Biomimetics 8, 95.

Kiakojouri, F., De Biagi, V., Chiaia, B., Sheidaii, M.R., 2020a. Progressive collapse of framed building structures: Current knowledge and future prospects. Eng. Struct. 206, 110061.

Kiakojouri, F., De Biagi, V., Chiaia, B., Sheidaii, M.R., 2022. Strengthening and retrofitting techniques to mitigate progressive collapse: A critical review and future research agenda. Eng. Struct. 262, 114274.

Kiakojouri, F., Sheidaii, M., 2018. Effects of finite element modeling and analysis techniques on response of steel moment-resisting frame in dynamic column removal scenarios. Asian J. Civ. Eng. 19, 295–307.

Kiakojouri, F., Sheidaii, M., De Biagi, V., Chiaia, B., 2020b. Progressive collapse assessment of steel moment-resisting frames using static-and dynamic-incremental analyses. J. Perform. Constr. Facil. 34, 04020025.

Kiakojouri, F., Sheidaii, M.R., De Biagi, V., Chiaia, B., 2021. Blast-induced progressive collapse of steel moment-resisting frames: Numerical studies and a framework for updating the alternate load path method. Eng. Struct. 242, 112541.

Kiakojouri, F., Zeinali, E., Adam, J.M., De Biagi, V., 2023a. Experimental studies on the progressive collapse of building structures: A review and discussion on dynamic column removal techniques. Structures 57, 105059.

Kim, J., Kim, T., 2009. Assessment of progressive collapse-resisting capacity of steel moment frames. J. Constr. Steel Res. 65, 169–179.

Kordbagh, B., Mohammadi, M., 2017. Influence of seismicity level and height of the building on progressive collapse resistance of steel frames. Struct. Des. Tall Special Build. 26, e1305.

Lalkovski, N., Starossek, U., 2022. The total collapse of the twin towers: What it would have taken to prevent it once collapse was initiated. J. Struct. Eng. 148, 04021276.

Lan, D.-Q., Jin, L., Qian, K., Zhang, R.-B., Li, J., 2023. Progressive collapse resistance of rc frames subjected to localized fire. J. Build. Eng. 79, 107746.

Liu, B., Soares, C.G., 2019. Effect of strain rate on dynamic responses of laterally impacted steel plates. Int. J. Mech. Sci. 160, 307–317.

Luu, V.-T., Kim, S.-E., 2023. An advanced beam–column element for analysis of frames in fires. Int. J. Mech. Sci. 260, 108650.

M. Musavi, Z., Sheidaii, M.R., 2021. Effect of seismic resistance capacity of moment frames on progressive collapse response of concentrically braced dual systems. Asian J. Civ. Eng. 22, 23–31.

Makoond, N., Setiawan, A., Buitrago, M., Adam, J.M., 2024. Arresting failure propagation in buildings through collapse isolation. Nature 629, 592–596.

Qiao, H., Chen, Y., Wang, J., Chen, C., 2020. Experimental study on beam-to-column connections with reduced beam section against progressive collapse. J. Constr. Steel Res. 175, 106358.

Shan, L., Petrone, F., Kunnath, S., 2019. Robustness of rc buildings to progressive collapse: Influence of building height. Eng. Struct. 183, 690–701.

Song, L., Hu, H., He, J., Chen, X., Tu, X., 2021. Collapse behaviour of a concrete-filled steel tubular column steel beam frame under impact loading. Adv. Mater. Sci. Eng. 2021, 6637014.

Stephen, D., Lam, D., Forth, J., Ye, J., Tsavdaridis, K.D., 2019. An evaluation of modelling approaches and column removal time on progressive collapse of building. J. Constr. Steel Res. 153, 243–253.

Tavakoli, H., Kiakojouri, F., 2013. Numerical study of progressive collapse in framed structures: A new approach for dynamic column removal. Int. J. Eng. Trans. Basics 26, 685–692.

Tavakoli, H., Kiakojouri, F., 2015. Threat-independent column removal and fire-induced progressive collapse: Numerical study and comparison. Civ. Eng. Infrastructures J. 48, 121–131.

Vamvatsikos, D., Cornell, C.A., 2002. Incremental Dynamic Analysis, Earthquake Engineering & Structural Dynamics. vol. 31, pp. 491–514.

Ventura, A., De Biagi, V., Chiaia, B., 2017. Effects of rockfall on an elastic–plastic member: A novel compliance contact model and dynamic response. Eng. Struct. 148, 126–144.

Wang, J., Wang, W., 2022. Macromodeling approach and robustness enhancement strategies for steel frame buildings with composite slabs against column loss. J. Struct. Eng. 148, 04021238.

Wang, J., Wang, W., Lehman, D., Roeder, C., 2019. Effects of different steel-concrete composite slabs on rigid steel beam–column connection under a column removal scenario. J. Constr. Steel Res. 153, 55–70.

Wang, F., Yang, J., Pan, Z., 2020. Progressive collapse behaviour of steel framed substructures with various beam–column connections. Eng. Fail. Anal. 109, 104399.

Xiang, S., He, Y., Golea, T., Denoël, V., Demonceau, J.-F., 2024. Simplified methods to predict the robustness of steel parking-structure joints. J. Constr. Steel Res. 213, 108355.

Xiao, W., Andrae, M., Gebbeken, N., 2020. Air blast tnt equivalence concept for blast-resistant design. Int. J. Mech. Sci. 185, 105871.

Yang, X.-J., Lin, F., Gu, X.-L., 2023. Progressive collapse resistance of rc beam–slab substructure under two-adjacent-edge-columns removal scenario. J. Build. Eng. 80, 108115.

Yin, Y., Wang, Y., 2005. Analysis of catenary action in steel beams using a simplified hand calculation method, Part 1: theory and validation for uniform temperature distribution. J. Constr. Steel Res. 61, 183–211.

Yong, A.C., Lam, N.T., Menegon, S.J., 2022. Collision Actions on Structures. CRC Press.

Yong, A.C., Lam, N.T., Menegon, S.J., Gad, E.F., 2020. Experimental and analytical assessment of flexural behavior of cantilevered rc walls subjected to impact actions. J. Struct. Eng. 146, 04020034.

Zhang, J.-Z., Jiang, B.-H., Feng, R., Chen, R., 2020. Robustness of steel moment frames in multi-column-removal scenarios. J. Constr. Steel Res. 175, 106325.